(*R*)-*N*-[^{11}C]Methyl-3-Pyrrolidyl Benzilate, a High-Affinity Reversible Radioligand for PET Studies of the Muscarinic Acetylcholine Receptor

MARC B. SKADDAN, DOUG M. JEWETT, PHIL S. SHERMAN, AND MICHAEL R. KILBOURN*
Department of Radiology, University of Michigan Medical School, Ann Arbor, Michigan 48109-0552

KEY WORDS *R*-*N*-[^{11}C]Methyl-3-pyrrolidyl benzilate; muscarinic acetylcholine receptor; phenserine; positron emission tomography

ABSTRACT We recently reported the synthesis and binding affinity of ligands for the muscarinic acetylcholine receptor (mAChR) based on both the pyrrolidyl and piperidyl benzilate scaffold. One of these, (*R*)-3-pyrrolidyl benzilate, was successfully radiolabeled with [^{11}C]methyl triflate and the resulting compound, (*R*)-*N*-[^{11}C]methyl-3-pyrrolidyl benzilate (3-[^{11}C]NMPYB), was evaluated as a reversible, acetylcholine-sensitive tracer for the mAChR (K_i of unlabeled 3-NMPYB is 0.72 nM). This compound displayed high, receptor-mediated retention in regions of the mouse and rat brain known to have high concentrations of mAChRs. Moreover, bolus studies in a pigtail monkey showed that this compound had superior clearance from the brain when compared to muscarinic radiotracers previously employed in human PET studies. Infusion studies in the same monkey revealed that it was possible to achieve equilibrium of radiotracer distribution for 3-[^{11}C]NMPYB in both the striatum and cortex. Sensitivity to endogenous acetylcholine levels was evaluated by injecting phenserine (5 mg/kg) into rats prior to administration of 3-[^{11}C]NMPYB in an equilibrium infusion protocol. This pretreatment produced a modest, statistically significant decrease (9–11%) in the distribution volume ratios for muscarinic receptor rich regions of the rat brain as compared to controls. **Synapse 45:31–37, 2002.**

INTRODUCTION

The link between cholinergic dysfunction and Alzheimer's disease (AD) has now been well documented. Changes of cholinergic function in AD include decreases in choline acetyltransferase (Aubert et al., 1992; Kuhl et al., 1999; Mash et al., 1985; Nordberg and Winblad, 1986; Perry et al., 1977), acetylcholinesterase (Geula and Mesulam, 1994; Gsell et al., 1996; Kuhl et al., 1999; Smith et al., 1988), high-affinity choline uptake (Rodriguez-Puertas et al., 1994; Rylett et al., 1983), and vesicular acetylcholine transporters (Efange et al., 1997; Kuhl et al., 1996, 1999). Alterations of numbers of the muscarinic acetylcholine receptor (mAChR), a G-protein coupled receptor involved in the regulation of higher cognitive functions such as memory and learning, have been described in some studies (Caulfield et al., 1982; Fisher, 1999; Mash et al., 1985; Nordberg and Winblad, 1986; Rodriguez-Puertas et al., 1997) but these changes are more ambiguous. Taken together, these changes in receptors, enzymes, and transporters of the cholinergic system have led to the hypothesis that enhancement of the cholinergic function using mAChR agonists or acetylcholinesterase (AChE) inhibitors can lead to amelioration of AD symptoms (review: Nordberg, 1999). While numerous cholinergic drugs (AChE inhibitors, acetylcholine (ACh)-releasing agents, and cholinergic agonists) have been developed for this purpose and several are in routine clinical use, relatively little is known of how these drugs affect muscarinic cholinergic receptor occupancy by ACh.

The in vivo imaging of mAChR availability using positron emission tomography (PET) or single photon

Contract grant sponsor: the Department of Energy; contract grant number: DE-FG02-ER60561; contract grant sponsor: the National Institutes of Health; contract grant number: T-32-CA09015.

*Correspondence to: Michael R. Kilbourn, Ph.D., Department of Radiology, University of Michigan Medical School, B1G412 University Hospital, Ann Arbor, MI 48109-0028. E-mail: mkilbour@umich.edu

Received 21 November 2001; Accepted 15 February 2002

DOI 10.1002/syn.10079

emission computed tomography (SPECT) offers an attractive opportunity for evaluating new or existing pharmaceutical approaches to enhancing the cholinergic system, provided a radiopharmaceutical with demonstrated sensitivity to ACh levels was available. Although numerous mAChR radiopharmaceuticals have been developed (Dannals et al., 1988; Dewey et al., 1990; Eckelman et al., 1985; Farde et al., 1996; Frey et al., 1992; Koeppe et al., 1994; Mulholland et al., 1995; Wilson et al., 1989, 1991), relatively few have been designed for the express purpose of measuring changes in endogenous ACh. Recently, Carson et al. (1998) reported sensitivity of the agonist [^{18}F]FP-TZTP (3-(3-(3-fluoropropyl)thio)-1,2,5-thiadiazol-4-yl)-1,2,5,6-tetrahydro-1-methylpyridine) to physostigmine-induced changes of ACh levels in monkey brain. Tsukada and co-workers also reported recently the sensitivity of two carbon-11 labeled piperidinyl benzilates, (+)-3-N-[^{11}C]ethylpiperidinyl benzilate (3-EtPB) and (+)-3-N-[^{11}C]propylpiperidinyl benzilate (3-PPB), to alterations of ACh levels in conscious monkey brain following pretreatment with the AChE inhibitor Aricept (Nishiyama et al., 2001). In rats, we have described the sensitivity of 4-[^{18}F]fluoroethylpiperidinyl benzilate (4-[^{18}F]FEPB) to changes of brain ACh levels following pretreatment with the AChE inhibitor phenserine (Skaddan et al., 2001). However, this last radiotracer proved difficult to apply in an equilibrium infusion protocol in monkeys due to metabolite issues (Skaddan and Kilbourn, unpublished results).

We describe here the radiochemical synthesis of (*R*)-*N*-[^{11}C]methyl-3-pyrrolidyl benzilate (3-[^{11}C]NMPYB), and the evaluation of this new mAChR radioligand in rodent and primate brain. The sensitivity of 3-[^{11}C]NMPYB to endogenous ACh levels has been examined by pretreatment of rats with phenserine (5 mg/kg) and injection of 3-[^{11}C]NMPYB in a bolus plus infusion (equilibrium distribution) protocol. Finally, this new radioligand has been evaluated as a reversible radiotracer suitable for equilibrium infusion PET studies of mAChR availability in the primate brain.

MATERIALS AND METHODS

Synthesis of 3-[^{11}C]NMPYB

No-carrier-added [^{11}C]CO_2 was prepared by proton irradiation of a nitrogen gas target [^{14}N(p,α)^{11}C] and converted sequentially to [^{11}C]methyl iodide and [^{11}C]methyl triflate (Jewett, 1992). 3-[^{11}C]NMPYB was produced by reacting [^{11}C]methyl triflate with the desmethyl precursor (1 mg) in 46 μL of dimethylacetamide. After complete transfer of the [^{11}C]methyl triflate the reaction was diluted with 1 mL cyclohexane and transferred to a neutral alumina column (4 × 110 mm). After washing the column with another 10 mL cyclohexane, 3-[^{11}C]NMPYB (**2**) was eluted with 1.5% methanol/dichloromethane. The main portion of radioactivity eluted at 10–13 mL. The collected portion was evaporated under nitrogen and reformulated with 10% ethanol/sterile water. For monkey studies, the final formulation was passed through a 0.22 μm pore size filter.

Reversed-phase quality control HPLC analyses were performed on a system consisting of a Beckman 110B isocratic pump, a Hitachi L-4000H UV detector (220 nm), a Beckman Model 120 radioisotope detector, and a Phenomenex C-8 (5 μm, 4.6 × 250 mm) analytical column. The mobile phase was 75% acetonitrile/0.05M NH_4OAc, with a flow rate of 1 mL/min.

To determine the lipophilicity of **2,** an 80 μCi sample was added to a premixed suspension of 2 mL octanol and 2 mL phosphate-buffered saline (PBS, pH 7.4). The resulting solution was vortexed for 2 min and centrifuged at 2,000 rpm for 5 min. An 800 μL aliquot of the octanol layer was transferred to a test tube containing 800 μL PBS. The solution was mixed and centrifuged as before. A 500 μL aliquot of the octanol layer was removed and extracted with 500 μL PBS as before. The radioactivity of each layer of the extractions was measured. Each octanol and water layer was weighed. The partition coefficient was calculated as the ratio of cpm/g of octanol to cpm/g of PBS per extraction. The average log $P_{o/w}$ of the three extractions for **2** is reported.

In vivo tissue distribution studies

The time-dependent regional brain distribution of radioactivity was determined in female CD1 mice (20–25 g, Charles River Laboratories) using a protocol approved by the University of Michigan Committee on Care and Use of Animals. Under diethyl ether anesthesia, animals were injected with 211–349 μCi of **2** via the tail vein, allowed to waken, and groups of animals sacrificed at various times after injection. The brains were quickly removed and dissected into regions of interest. Blood samples and for certain time points heart and bone (femur) samples were also obtained. Tissue samples were counted for carbon-11 and then weighed. Radioactivity retention for each region was calculated as %ID/gram tissue. To ascertain whether the uptake was receptor-mediated, sets ($n = 4$) of animals were administered scopolamine (5 mg/kg, i.p.) or unlabeled **2** (5 mg/kg, i.p.) 15 min prior to administration of the radiopharmaceutical.

Equilibrium regional brain distribution were determined in male CD rats (200–250 g, Charles River Laboratories). Under sodium pentobarbitol anesthesia, an infusion line was surgically inserted and secured in one femoral vein. The rats were restrained (plastic tubes) and allowed to waken. Radiotracer infusions were done using a Harvard programmable infusion pump which administered **2** (4.02 ± 1.07 mCi) as a bolus of 1 mL delivered over 1 min followed by a constant infusion of the remaining 0.5 mL over a period of 79 min. At the end of the infusion animals were sacrificed with sodium

pentobarbitol overdose and the brains were removed and dissected into regions of interest (ROIs). Tissue samples were counted for carbon-11 and then weighed. Radioactivity retention for each region was calculated as %ID/gram tissue.

Studies of the effects of pretreatment with phenserine (5 mg/kg i.p., administered 30 min prior) were done in rats using the bolus + infusion protocol.

Monkey PET imaging

The primate PET imaging studies were conducted in a female pigtail monkey (*Macaca nemistrina*) weighing 8.3 kg. Imaging was done using TCC 4600A three-ring, five-slice PET camera, modified with custom collimation to provide an in-plane resolution of 7.5 mm FWHM. The primate was anesthetized (15 mg/kg i.m. ketamine and 2 mg/kg i.m. xylazine, repeated as necessary) and intubated to prevent aspiration of salivary secretions. An $[^{15}O]H_2O$ scan was performed to verify the position of the monkey brain within the scanner field of view. The bolus study was initiated with an i.v. injection of 26 mCi of **2.** For the equilibrium infusion studies ($n = 2$) involving **2,** 50% of the total activity (total doses of 53.9, 50.0 mCi) was administered as a bolus during the first minute using a Harvard programmable infusion pump and the remaining 50% was infused at a constant rate over the next 89 min. For all studies kinetic data were acquired using a 20 frame acquisition sequence which lasted 90 min (five frames of 1 min duration, 17 frames at 5 min/frame for the remaining 85 min). A mathematical attenuation correction was applied in image reconstruction. ROIs were drawn around the frontal/temporal cortex and around each striatum and these regions applied to all images in the sequence to generate tissue time–activity curves.

Rodent metabolite studies

In vivo metabolism studies were carried out in female CD1 mice (25–30 g, Charles River Laboratories). Under diethyl ether anesthesia, animals were injected with **2** (1.2 mCi/mouse) via the tail vein, allowed to waken, and sacrificed at various times after injection (one animal per time point). Whole mouse brain was placed in a polystyrene tube containing 1 mL ethanol, then homogenized. Blood (500 μL) was also removed and placed in a 1.5 mL Eppendorf tube containing 750 μL ethanol, then shaken. The blood and brain tubes were centrifuged at 3,500 rpm for 5 min and the supernatant was spotted (3×5 μL) onto glass silica TLC plates (vide supra). The spots were dried by heating the back of the plate with a heat gun for 15–20 sec. After cooling, the plates were developed in a chamber containing 5% methanol/dichloromethane. The chamber was also saturated with NH_3 by placing a vial inside containing concentrated NH_4OH. After the plates were developed they were removed, air-dried, and radioactivity was visualized using a Fuji phosphorimaging system. ROIs corresponding to the authentic radiotracer, radioactive metabolite, and chromatographic origin were drawn by hand on these images. An additional ROI was drawn in a blank area of the plate to serve as a background correction and the optical density for each ROI was quantified. The fraction of authentic radiotracer at each time point was calculated as the optical density of the authentic tracer ROI divided by the total signal in all regions and was converted to a percentage.

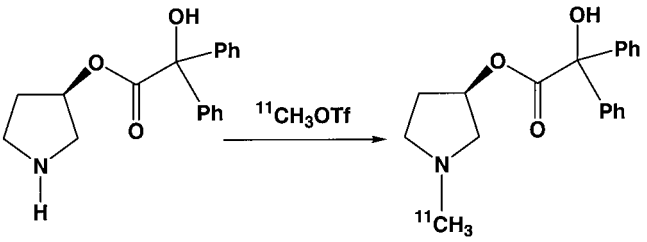

Fig. 1. Synthesis of 3-[11C]NMPYB (**2**).

Statistics

Statistical significance of drug pretreatments was evaluated using an unpaired Student's t-test. $P < 0.05$ was considered significant.

RESULTS

The radiochemical synthesis of **2** proceeded a via alkylation of the nor-precursor with [11C]methyl triflate, using dimethylacetamide as the solvent (Fig. 1). The reaction is extremely rapid, reproducible, and reliable and the desired product can be purified by simply passing the reaction contents through a short neutral alumina column, thus eliminating the need for HPLC purification. Typical results for a 25-min, 20-μA irradiation target irradiation were >350 mCi of **2** in ≥96% radiochemical purity. Overall synthesis times were 15–20 min from end-of-bombardment, but synthesis times and yields were not optimized. Apparent specific activities from HPLC analysis were on the order of 1,500–3,000 Ci/mmol, with only trace amounts (<1 μg/mL) of nor-precursor **1** present in the final solution.

The time-dependent in vivo tissue distribution of **2** in mouse brain is summarized in Table I. Uptake in the brain was highest in the striatum, cortex, and hippocampus and lowest in the hindbrain, which corresponds well to known regional brain concentrations of mAChRs (Lee et al., 1995; Lin et al., 1986; Snyder et al., 1975). Blocking doses of the mAChR antagonist scopolamine at the 20-min timepoint resulted in significant decreases in striatal (−84%) and cortical (−75%) radioactivity concentrations. Significant decreases (65–75%) were observed when blocking studies were carried out with unlabeled **2** ($K_i = 0.72$ nM). These

*TABLE I. Tissue distribution (%ID/gram) of **2** in female CD1 mice*

Tissue	%ID/gram ± SD, $n = 4$				
	2 min	20 min[a]	20 min block scopolamine[b]	20 min block **2**[b]	60 min
Striatum	11.30 ± 1.74	15.04 ± 1.28	2.43 ± 0.85	3.92 ± 0.90	11.04 ± 1.87
Cortex	11.41 ± 1.51	12.91 ± 0.81	3.20 ± 0.92	4.61 ± 0.87	8.72 ± 0.46
Cerebellum	7.70 ± 1.21	2.94 ± 0.28	2.36 ± 0.65	3.15 ± 0.55	1.49 ± 0.12
Hippocampus	11.79 ± 1.64	12.53 ± 1.10	3.25 ± 0.93	4.36 ± 0.75	9.03 ± 0.46
Hypothalamus	11.91 ± 1.36	7.78 ± 1.68	2.34 ± 0.70	3.40 ± 0.71	3.99 ± 0.50
Thalamus	10.89 ± 1.46	7.62 ± 1.26	2.30 ± 0.69	2.88 ± 0.42	3.20 ± 0.23
Pons/medulla	9.10 ± 1.04	5.52 ± 0.61	2.37 ± 0.66	3.19 ± 0.57	2.27 ± 0.08
Rest of brain	9.90 ± 1.83	7.84 ± 1.21	2.32 ± 0.60	3.27 ± 0.57	4.21 ± 0.27
Heart	9.30 ± 1.18	2.36 ± 0.72	N/A	N/A	1.78 ± 0.09
Blood	1.57 ± 0.11	1.58 ± 0.03	1.55 ± 0.19	1.76 ± 0.07	1.60 ± 0.12
Striatum/cereb.	1.49 ± 0.18	5.16 ± 0.62	1.01 ± 0.18	1.23 ± 0.15	7.42 ± 1.27
Cortex/cereb.	1.49 ± 0.13	4.42 ± 0.35	1.35 ± 0.08	1.46 ± 0.03	5.87 ± 0.22

[a] $n = 8$.
[b] 5 mg/kg.

findings demonstrate that uptake in the receptor-rich regions of the brain was mAChR-mediated.

In the equilibrium infusion studies in rats a similar pattern of distribution was evident (striatum > cortex > hippocampus > hypothalamus, thalamus > cerebellum), but smaller region/cerebellum ratios were obtained (Fig. 1). This was not surprising, as we and others have described significantly different tissue concentration ratios following bolus and equilibrium radiotracer distributions (Kilbourn and Sherman, 1997). These ratios obtained at equilibrium, which represent distribution volume ratios and are directly proportional to the binding potential of the tissues (DVR = BP +1), are a widely used and more accepted estimate of specific binding than tissue ratios obtained at a single time point following bolus radiotracer injection. Sensitivity of the equilibrium specific binding measures to changes in endogenous acetylcholine levels was studied using pretreatment with phenserine (a potent AChE-inhibitor [Grieg et al., 1995]) or saline 30 min prior to infusion of **2.** The dose of phenserine chosen (5 mg/kg) significantly inhibits brain acetylcholinesterase (Kilbourn et al., 1999). Inhibition of AChE by phenserine produced a statistically significant decrease in the distribution volume ratio for the striatum (−9%, $P = 0.03$), cortex (−11%, $P = 0.02$), and hippocampus (−10%, $P = 0.01$) following phenserine pretreatment (Fig. 2). These decreases were due entirely to changes in radioligand binding to these regions and not because of increased uptake or retention in the cerebellum (the reference region), as radioactivity concentrations in that region of the brain remained unchanged throughout all of the studies (controls, 0.17 ± 0.01% injected dose/g; phenserine, 0.17 ± 0.05% injected dose/g).

The regional tissue time–activity curves (TAC) of **2** following a bolus injection into a monkey is shown in Figure 3. The time–activity curves of cortical uptake and clearance in monkey brain for the structurally related muscarinic radiotracers 4-[^{11}C]NMPB and [^{18}F]FEPB are shown for comparison. All of these benzilate esters are moderately lipophilic and show high

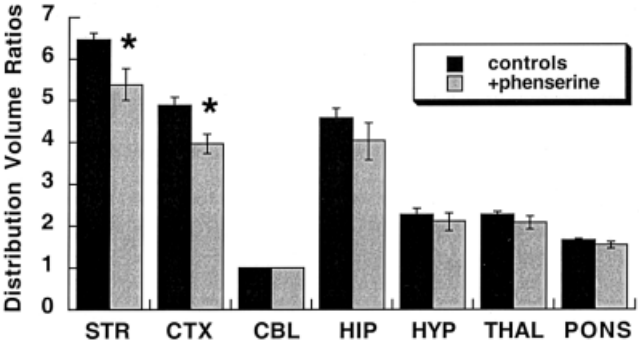

Fig. 2. Comparison of regional brain 3-[^{11}C]NMPYB distribution volume ratios between control and phenserine-treated male rats. Rats were injected with either saline ($n = 8$, controls) or phenserine (5 mg/kg: $n = 8$) 30 min prior to beginning the injection of 3-[^{11}C]NMPYB in a bolus plus infusion protocol for 80 min. Distribution volume ratios (DVRs) are ratios of concentrations of radioactivity in ROIs relative to the cerebellum, presented as mean ± SD. *$P < 0.05$ vs. controls.

early uptake into brain tissues. Clearance of **2** from the cortex is more rapid than that of 4-[^{11}C]NMPB but not as fast as the fluorinated derivative. This agrees well with the 10-fold lower muscarinic receptor binding affinity reported for unlabeled 3-NMPYB vs. 4-NMPB (Skaddan et al., 2000). The kinetics of **2** compare more favorably to [^{18}F]FEPB, a compound we have shown to be a reversible, ACh-sensitive muscarinic agent in rats (Skaddan et al., 2001a).

The tissue radioactivity curves for **2** in monkey brain following a bolus + infusion is presented in Figure 4. With a bolus to infusion ratio of 50:50, the time–activity curves of the striatum and cortex reach a plateau by 50 min into the infusion. Thus, it is possible not only to achieve equilibrium distributions of **2** in rodents, but in monkey brain as well. Distribution volume ratios (DVRs) in the monkey brain, calculated as ratios of equilibrium concentrations in ROIs to cerebellum, were 3.52 ± 0.18 for the striatum and 2.70 ± 0.10 for the cortex for 50–90 min (average for nine consecutive 5-min PET scans of one study). Reversibility of the

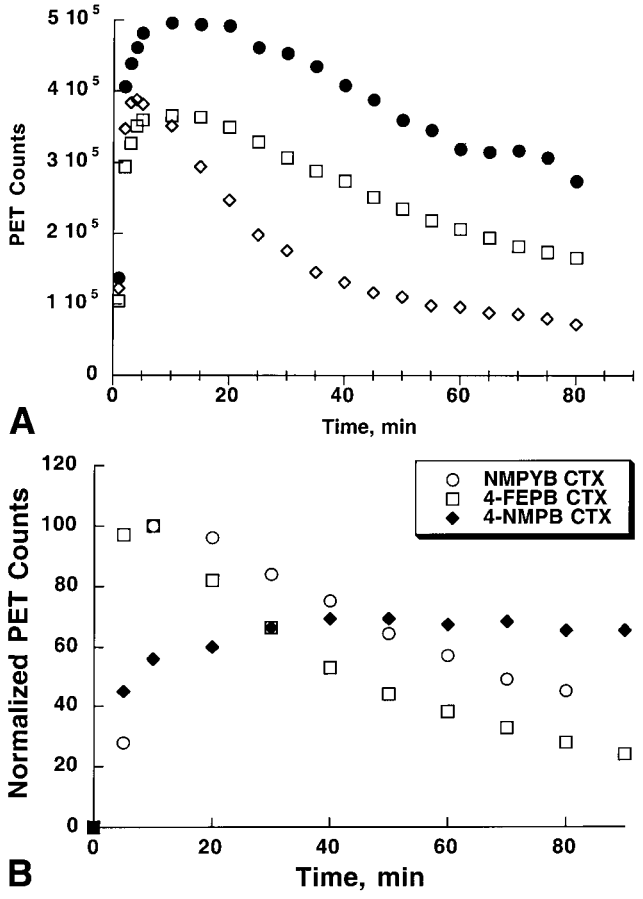

Fig. 3. **A:** Tissue time–activity curves in monkey brain for striatum, cortex and cerebellum following bolus injection of 3-[11C]NMPYB. **B:** Comparison of cortical time–activity curves for 3-[11C]NMPYB with the structurally related radioligands 4-[11C]NMPB and 4-[18F]FEPB. Data has been normalized to account for differences in injected doses.

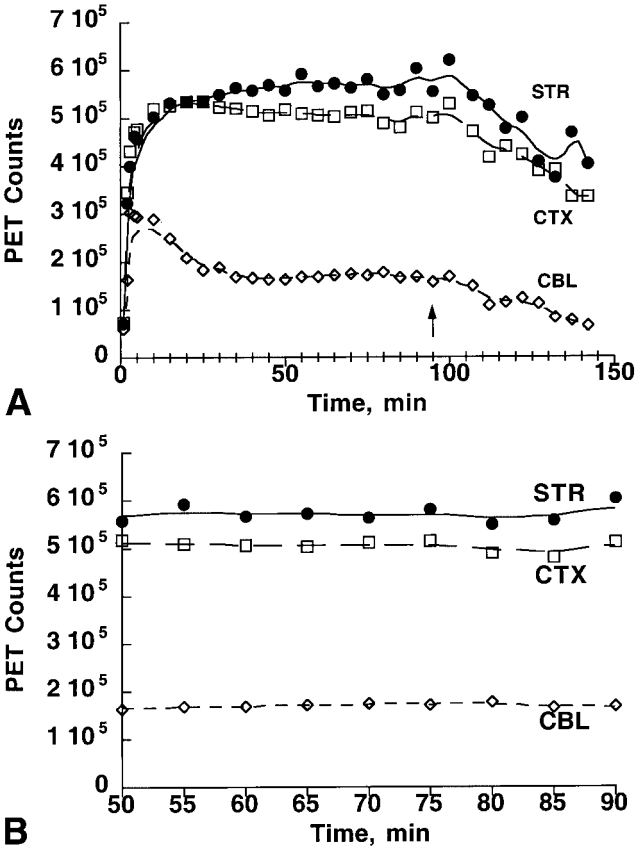

Fig. 4. **A:** Time–activity curves of monkey cortex and striatum following injection of 3-[11C]NMPYB using a bolus plus infusion protocol. The arrow indicates the time point at which radiotracer administration was stopped and radioactivity began washing out of brain regions. **B:** Tissue time–activity curves for the time period 50–90 min, demonstrating constant tissue concentrations of radioactivity during the later stages of the constant infusion period of a bolus + infusion protocol.

binding of 3-[11C]NMPYB could be clearly demonstrated by following the rapid washout of radioactivity from all brain regions following the end of the constant infusion of the radiotracer (Fig. 4A). The rapid, reversible kinetics of 3-[11C]NMPYB are a significant improvement over the previous carbon-11 labeled mAChR radioligands we have previously introduced into clinical PET imaging, namely [11C]scopolamine, [11C]tropanyl benzilate, and 4-[11C]NMPB, none of which were applicable to an equilibrium infusion protocol.

Limited metabolite studies of **2** in mice were performed since the metabolic profile of this class of compounds has already been extensively covered (Hüller et al., 1988; Kiesewetter et al., 1997; Mulholland et al., 1992; Nishiyama et al., 2001; Skaddan et al., 2001b; Tsuda et al., 1991; Tsukada et al., 2001). As with most of the amine benzilates, **2** is rapidly metabolized in vivo, with 80% authentic (R_F = 0.74) remaining after 2 min, 35% after 20 min, and 13% after 40 min in whole mouse blood. The major metabolites remained at the baseline with the mobile phase used and therefore would not be expected to cross the blood–brain barrier. Indeed, after 20 min 97% of the TLC activity from whole brain extracts was associated with authentic **2.**

DISCUSSION

The advantage of infusing a radioligand to equilibrium over traditional bolus techniques is that it provides an excellent method of determining distribution volume ratios (DVRs, the ratio of radioactivity in regions of the brain with high concentrations of muscarinic receptors to regions with low or no concentration of receptors), an in vivo estimate of specific binding which is proportional to the numbers of available binding sites and which can be obtained independent of changes in radiotracer metabolism or delivery (i.e., blood flow) (Carson et al., 1998). In contrast to many previous radioligands we have evaluated as PET radiotracers for the mAChR, such as [11C]scopolamine, [11C]tropanyl benzilate, and 4-[11C]N-methylpiperidinyl benzilate (4-NMPB), the radioligand developed here ([11C]NMPyB) is rapidly reversible and thus can

be successfully infused to equilibrium distributions in rodent and primate brain within acceptable time frames (<60 min). ([^{11}C]NMPyB also differs in pharmacokinetics and sensitivity to endogenous acetylcholine as compared to recently developed radioiodinated ligands for SPECT such as [^{123}I]IQNP, which requires long imaging times (48 h) to reach peak equilibrium and which have not been shown to be sensitive to endogenous neurotransmitter (Nobuhara et al., 2001).

According to the occupancy model for radiotracer-endogenous ligand competition, increases or decreases in ACh levels should lead to lower or higher DVR, respectively. The decreases observed here in the rat brain following AChE inhibition show that **2** follows the classic occupancy model radioligand behavior, similar to that reported for the structurally related N-ethyl (3-EtPB) and N-propyl piperidinyl benzilates (3-PPB) (Nishiyama et al., 2001). The decreases in radioligand binding observed in our study (9–10%) and others (12–18%; Nishiyama et al., 2001) are modest when compared to the orders of magnitude changes in ACh concentrations induced by such AChE inhibitors as phenserine or Aricept. However, relatively small changes in receptor-based radiotracer occupancy in response to extremely high alterations in endogenous neurotransmitter is often the norm in these types of experiments (Laruelle, 2000).

The relationships between in vitro affinity of mAChR ligands, specificity of in vivo binding, and sensitivity to endogenous acetylcholine remain ambiguous, although the available data does suggest that lower-affinity compounds are more sensitive. Strict comparisons of the available literature data are made more difficult, as in vitro binding affinities for the identical compounds can vary by more than 20-fold in data from different laboratories, the in vivo studies have been done in both rodents and primates, and data analyses done using different pharmacokinetic modeling approaches. The greatest sensitivity appears to reside in the compounds with the poorer in vitro binding affinities, such as the propyl derivative 3-PPB and the fluoroethyl derivative 4-FEPB. In our prior in vitro assays of these two compounds we found very similar K_i values (3-PPB, 1.88 nM; 4-FEPB, 1.83 nM) for inhibition of [^{3}H]scopolamine binding; in contrast, Nishiyama et al. (2001) report a K_i value of 47 nM for 3-PPB, using [^{3}H]quinuclidinyl benzilate as radioligand in the in vitro assay. The reasons for this discrepancy are not evident. No sensitivity to acetylcholinesterase pretreatment was previously shown (Nishiyama et al., 2001) for the very high-affinity N-methyl compound 4-NMPB (K_i = 0.07 nM; Skaddan et al., 2000). The compounds with intermediate affinities such as the pyrrolidinyl derivative 4-NMPyB (K_i 0.72 nM), studied here, and the N-ethyl derivative 3-EtPB (K_i 12.9 nM by Nishiyama et al. [2001] and K_i 1.46 nM by Skaddan et al. [2000]) show small sensitivities to changes of endogenous acetylcholine. Thus, as in other receptor systems (Laruelle, 2001), it remains difficult to predict the sensitivity of a radiotracer to changes of endogenous competitor neurotransmitter based simply on the equilibrium in vitro binding affinity. Our preliminary attempts to alter the in vivo binding of [^{11}C]NMPyB in the primate brain, using administration of acetylcholinesterase inhibitors, have proven unsuccessful. It is not clear if this was due to the affinity of our new radioligand [^{11}C]NMPyB or a result of insufficient increases of the endogenous acetylcholine levels in the primate brain; further studies are needed. Even more perplexing are the opposite behaviors of closely related compounds such as [^{18}F]FEPB and [^{11}C]EPB (and [^{11}C]NMPyB), although it can be hypothesized that the fluoroethyl substituent induces a significant physiochemical change in the ligand: addition of a fluoroethyl group has been shown to decrease the pK_a of pyrrolidyl amines in dopaminergic benzamides by as much as 100-fold (Schmidt et al., 1994). How such a change results in differential binding of ligands, perhaps to internalized vs. externalized muscarinic receptors, remains to be determined.

ACKNOWLEDGMENTS

The authors thank the cyclotron staff and radiochemistry staff of the Division of Nuclear Medicine, University of Michigan Medical School, for production of the radioisotope. Special thanks to Dr. Robert Koeppe for discussions of primate kinetics, Dr. Kirk Frey for discussions regarding muscarinic receptor pharmacology, and Kyle Kuszpit and Leslie Doherty for assistance in the animal studies.

REFERENCES

Aubert I, Araujo DM, Cecyne D, Robitaille Y, Gauthier S, Quirion R. 1992. Comparitive alterations of nicotinic and muscarinic binding sites in Alzheimer's and Parkinson's disease. J Neurochem 58:529–541.

Carson RE, Kiesewetter DO, Jagoda E, Der MG, Herscovitch P, Eckelman WC. 1998. Muscarinic cholinergic receptor measurements with [^{18}F]FP-TZTP: control and competition studies. J Cereb Blood Flow Metab 18:1130–1142.

Caulfield MP, Straughan DW, Cross AJ, Crow T, Birdsall NJ. 1982. Cortical muscarinic receptor subtypes and Alzheimer's disease. Lancet 2:1277–1285.

Dannals RF, Langstrom B, Ravert HT, Wilson AA, Wagner HN Jr. 1988. Synthesis of radiotracers for studying muscarinic cholinergic receptors in the living human brain using positron emission tomography. Appl Radiat Isot 39:291–295.

Dewey SL, Volkow ND, Logan J, MacGregor RR, Fowler JS, Schlyer DJ, Bendriem B. 1990. Age-related decreases in muscarinic cholinergic receptor binding in the human brain measured with positron emission tomography (PET). J Neurosci Res 27:569–575.

Eckelman WC, Eng R, Rzeszotarski WJ, Gibson RE, Francis B, Reba RC. 1985. Use of 3-quinuclidinyl 4-iodobenzilate as a receptor binding radiotracer. J Nucl Med 26:637–642.

Efange SM, Garland EM, Staley JK, Khare AB, Mash DC. 1997. Vesicular acetylcholine transporter density and Alzheimer's disease. Neurobiol Aging 18:407–413.

Farde L, Suhara T, Halldin C, Nyback H, Nakashima Y, Swahn C-G, Karlsson P, Ginovart N, Bymaster FP, Shannon HE, Foged C, Suzdak PD, Sauerberg P. 1996. PET study of the M1-agonists [^{11}C]xanomeline and [^{11}C]butylthio-TZTP in monkey and man. Dementia 7:187–195.

Fisher A. 1999. Muscarinic receptor agonists in Alzheimer's disease. CNS Drugs 12:197–214.

Frey KA, Koeppe RA, Mulholland GK, Jewett DM, Hichwa R, Ehrenkaufer RLE, Carey JE, Wieland DM, Kuhl DE. 1992. In vivo muscarinic cholinergic receptor imaging in human brain with [11C]scopolamine and positron emission tomography. J Cereb Blood Flow Metab 12:147–154.

Geula C, Mesulam M-M. 1994. Cholinergic systems and related neuropathological predilection patterns in Alzheimer disease. In: Terry RD, Katzman R, Bick KL, editors. Alzheimer disease. New York: Raven Press.

Grieg NH, Pei X-F, Soncrant DK, Brossi A. 1995. Phenserine and ring C hetero-analogues: drug candidates for the treatment of Alzheimer's disease. Med Res Rev 15:3–31.

Gsell W, Strein I, Riederer P. 1996. The neurochemistry of Alzheimer type, vascular type and mixed type dementias compared. J Neural Transm Suppl 47:73–101.

Hüller G, Haustein K-O, Scheithauer S. 1988. Studies on the metabolic pattern of propiverine in urine after single administration. Pharmazie 43:91–95.

Jewett DM. 1992. A simple synthesis of [11C]methyl triflate. Appl Radiat Isot 43:1383–1385.

Kiesewetter DO, Carson RE, Jagoda EM, Endres CJ, Der MG, Herscovitch P, Eckelman WC. 1997. In vivo muscarinic binding selectivity of (*R*,*S*)- and (*R*,*R*)-[18F]-fluoromethyl QNB. Biorg Med Chem 5:1555–1567.

Kilbourn MR, Sherman PS, Snyder SE. 1999. Simplified methods for in vivo measurement of acetylcholinesterase activity in rodent brain. Nucl Med Biol 26:543–550.

Koeppe RA, Frey KA, Mulholland GK, Kilbourn MR, Buck A, Lee KS, Kuhl DE. 1994. [11C]Tropanyl benzilate-binding to muscarinic cholinergic receptors: methodology and kinetic modeling alternatives. J Cereb Blood Flow Metab 14:85–99.

Kuhl DE, Minoshima S, Fessler JA, Frey KA, Foster NL, Ficaro EP, Wieland DM, Koeppe RA. 1996. In vivo mapping of cholinergic terminals in normal aging, Alzheimer's disease, and Parkinson's disease. Ann Neurol 40:399–410.

Kuhl DE, Koeppe RA, Minoshima S, Snyder SE, Ficaro EP, Foster NL, Frey KA, Kilbourn MR. 1999. In vivo mapping of cerebral acetylcholinesterase activity in aging and Alzheimer's disease. Neurology 52:691–699.

Laruelle M. 2000. Imaging synaptic neurotransmission with in vivo binding competition techniques: a critical review. J Cereb Blood Flow Metab 20:423–451.

Lee J, Paik CH, Kiesewetter DO, Park SG, Eckelman WC. 1995. Evaluation of stereoisomers of 4-fluoroalkyl analogues of 3-quinuclidinyl benzilate in in vivo competition studies for the M1, M2, and M3 muscarinic receptor subtypes in brain. Nucl Med Biol 22:773–781.

Lin S-C, Olson KC, Okazaki H, Richelson E. 1986. Studies on muscarinic binding sites in human brain identified with [3H]pirenzipine. J Neurochem 46:274–279.

Mash DC, Flynn DD, Potter LT. 1985. Loss of M2 muscarine receptors in the cerebral cortex in Alzheimer's disease and experimental cholinergic denervation. Science 228:1115–1117.

Mulholland GK, Otto CA, Jewett DM, Kilbourn MR, Koeppe RA, Sherman PS, Petry NA, Carey JE, Atkinson ER, Archer S, Frey KA, Kuhl DE. 1992. Synthesis, rodent distribution, dosimetry, metabolism, and monkey images of carbon-11-labeled (+)-2α-tropanyl benzilate: a central muscarinic receptor imaging agent. J Nucl Med 33:423–430.

Mulholland GK, Kilbourn MR, Sherman P, Carey JE, Frey KA, Koeppe RA, Kuhl DE. 1995. Synthesis, in vivo biodistribution and dosimetry of [11C]N-methylpiperidinyl benzilate ([11C]NMPB), a muscarinic acetylcholinergic-receptor antagonist. Nucl Med Biol 22:13–17.

Nishiyama S, Tsukada H, Sato K, Kakiuchi T, Ohba H, Harada N, Takahashi K. 2001. Evaluation of PET ligands (+)*N*-[11C]ethyl-3-piperidyl benzilate and (+)*N*-[11C]propyl-3-piperidyl benzilate for muscarinic cholinergic receptors: a PET study with microdialysis in comparison with (+)*N*-[11C]methyl-3-piperidyl benzilate in the conscious monkey brain. Synapse 40:159–169.

Nobuhara K, Farde L, Halldin C, Karlsson P, Swahn CG, Olsson H, Bergstrom KA, Larsson SA, Schnell PO, McPherson DW, Savonen A, Hiltunen J, Sedvall G. 2001. SPET imaging of central muscarinic acetylcholinergic receptors with iodine-123 labeled E-IQNP and Z-IQNP. Eur J Nucl Med 28:13–24.

Nordberg A. 1999. PET studies and cholinergic therapy in Alzheimer's disease. Rev Neurol (Paris) 155 (4S):53–63.

Nordberg A, Winblad B. 1986. Reduced number of [3H]nicotine and [3H]acetylcholine binding sites in the frontal cortex of Alzheimer brains. Neurosci Lett 72:115–119.

Perry EK, Perry RH, Gibson RH, Blessed G, Tomlinson BEA. 1977. Cholinergic connection between normal aging and senile dementia in the human hippocampus. Neurosci Lett 6:85–89.

Rodriguez-Puertas R, Pazos A, Zarranz JJ, Pascual J. 1994. Selective cortical decrease of high-affinity choline uptake carrier in Alzheimer's disease: an autoradiographic study using 3H-hemicholinium-3. J Neural Transm Park Dis Dement Sect 8:161–169 [erratum J Neural Transm Park Dis Dement Sect 1995;9(2–3):249].

Rodriguez-Puertas R, Pascual J, Vilaro T, Pazos A. 1997. Autoradiographic distribution of M1, M2, M3, and M4 muscarinic receptor subtypes in Alzheimer's disease. Synapse 26:341–350.

Rylett RJ, Ball MJ, Colhoun EH. 1983. Evidence for high affinity choline transport in synaptosomes prepared from hippocampus and neocortex of patients with Alzheimer's disease. Brain Res 289:169–175.

Schmidt DE, Votaw JR, Kessler RM, De Paulis T. 1994. Aromatic and amine substituent effects on the apparent lipophilicities of *N*-[(2-pyrrolidinyl)methyl]-substituted benzamides. J Pharm Sci 83:305–315.

Skaddan MB, Kilbourn MR, Snyder SE, Sherman PS, Desmond TJ. 2000. Synthesis, 18F-labeling, and biological evaluation of piperidyl and pyrrolidyl benzilates as in vivo ligands for muscarinic acetylcholine receptors. J Med Chem 43:4552–4562.

Skaddan MB, Kilbourn MR, Snyder SE, Sherman PS. 2001a. Acetylcholinesterase inhibition increases in vivo radioligand binding to muscarinic acetylcholine receptors. J Cereb Blood Flow Metab 21: 144–148.

Skaddan MB, Sherman PS, Kilbourn MR. 2001b. The role of species-dependent metabolism in the regional brain retention of 18F-labeled muscarinic acetylcholine receptor ligands. Nucl Med Biol 28:753–759.

Smith CJ, Perry EK, Perry RH, Candy JM, Johnson M, Bonham JR, Dick DJ, Fairbairn A, Blessed G, Birdsall NJ. 1988. Muscarinic cholinergic receptor subtypes in hippocampus in human cognitive disorders. J Neurochem 50:847–856.

Snyder SH, Chang KJ, Kuhar MJ, Yamamura HI. 1975. Biochemical identification of the mammalian muscarinic cholinergic receptor. Fed Proc 34:1915–1921.

Tsuda M, Yamamoto Y, Uda K, Shindo T, Kawaguchi Y. 1991. Pharmacokinetics of propiverine hydrochloride. (5). Animal species differences in vivo, in vitro and protein binding. Yakubutsu Dotai 6:3–20.

Tsukada H, Takahashi K, Miura S, Nishiyama S, Kakiuchi T, Ohba H, Sato K, Hatazawa J, Okudera T. 2001. Evaluation of novel PET ligands (+)*N*-[11C]methyl-3-piperidyl benzilate ([11C](+)3-MPB) and its stereoisomer [11C](−)3-MPB for muscarinic cholinergic receptors in the conscious monkey brain: a PET study in comparison with [11C]4-MPB. Synapse 39:182–192.

Wilson AA, Dannals RF, Ravert HT, Frost JJ, Wagner HN Jr. 1989. Synthesis and biological evaluation of [125I]- and [123I]-iodododexetimide, a potent muscarinic cholinergic receptor antagonist. J Med Chem 32:1057–1062.

Wilson AA, Scheffel UA, Dannals RF, Stathis M, Ravert HT, Wagner HN Jr. 1991. In vivo biodistribution of two [18F]-labelled muscarinic cholinergic receptor ligands: 2-[18F]- and 4-[18F]-fluorodexetimide. Life Sci 48:1385–1394.